Available at
www.ElsevierComputerScience.com
POWERED BY SCIENCE DIRECT®

Signal Processing 84 (2004) 919–942

SIGNAL PROCESSING

www.elsevier.com/locate/sigpro

Three-mode data set analysis using higher order subspace method: application to sonar and seismo-acoustic signal processing

Nicolas Le Bihan[a,*], Guillaume Ginolhac[b]

[a] *Laboratoire des Images et des Signaux, ENSIEG, CNRS UMR 5083, B.P. 46, 38402 Saint Martin d'Hères Cedex, France*
[b] *GEA, IUT Ville d'Avray, 1, Ch. Desvallières, 92410 Ville d'Avray, France*

Received 17 March 2003; received in revised form 9 January 2004

Abstract

In this paper, a three-mode subspace technique based on higher order singular value decomposition (HOSVD) is presented. This technique is then used in the context of wave separation. It can be regarded as the extension to three-mode arrays of the well-known subspace technique proposed by Eckart and Young (Psychometrica 1 (1936) 211) for matrices. Three-mode data sets are increasingly encountered in signal processing and are classically processed using matrix algebra techniques. The proposed approach aims to process naturally three-mode data with multilinear algebra tools. So in the proposed algorithms, the structure of the data set is preserved and no reorganization is performed on it. The choice of HOSVD for subspace method is explained, studying the rank definition for three-mode arrays and orthogonality between subspaces. A projector formulation for three-mode *signal* and *noise* subspaces is also given and the improvement of separation with the three-mode approach over a *componentwise* approach is shown. We study two applications for the proposed Higher Order Subspace approach: the reverberation problem in sonar, and the polarized seismo-acoustic wave separation problem. For the first application, we propose a three-mode version of the Principal Component Inverse algorithm (IEEE Trans. Aerospace Electron. Systems 30(1) (1994) 55). We apply the proposed technique on simulated data as well as on real sonar data where the three modes are angle, delay and distance. For the second application, we consider the polarization of the seismic wave as the third mode (in addition to time and distance modes) and show the resulting improvement of wave separation using the proposed Higher Order approach.

Keywords: Three-mode arrays; Subspace method; Three-mode array decomposition; Higher order singular value decomposition; Multimodal sonar images; Seismo-acoustic signal processing; Wave separation; Acoustic and elastic wavefield separation; Three-mode PCI

1. Introduction

Many application domains are faced with multimodal data, due to the increasing number of parameters collected by sensors or the dimensions of the physical system under study. Data with one or two modes are well understood as they can be modeled and processed respectively via vector and matrix approaches. Processing such data requires linear algebra techniques which have been largely studied for several years in signal and image processing.

* Corresponding author. Tel.: +33-4-76-82-64-86.
E-mail addresses: nicolas.le-bihan@lis.inpg.fr (N. Le Bihan), guillaume.ginolhac@cva.u-paris10.fr (G. Ginolhac).

0165-1684/$ - see front matter © 2004 Elsevier B.V. All rights reserved.
doi:10.1016/j.sigpro.2004.02.003

When dealing with data having more than two modes, difficulties soon arise because the well-known concepts of linear algebra do not necessarily extend to the N-mode case. For example, the estimation of the rank of a matrix can be performed using the singular value decomposition (SVD) [7], while the direct estimation (and so, the direct computation) of the rank of a multimodal array is not possible [8]. In most applications where N-mode ($N > 2$) data sets are encountered, classical signal processing techniques consist of reordering the data set in a matrix formulation [16,15]. The original data structure is then rebuilt after processing.

Such an approach is practical in that all operations are reduced to well-known matrix operations, but it may not be satisfactory from the point of view of the physical structure of the observed system. For example, an antenna array recording waves with polarization properties will lead to three-mode data set recording (see Section 4 for details). Reordering such data is often done despite the polarization mode. However, such an approach breaks the polarization "dimension", and does not take advantage of the physical type of the recorded waves.

In this paper, we show that keeping the structure of the data set during processing enhances the obtained results. This is demonstrated using a case study on the rank (along each mode) of the data set. Using the "mutual information" available on the modes of the data, makes it possible to decorrelate the different components of the recorded signal. In order to perform a decomposition and a rank study of three-mode data, we use the higher order singular value decomposition (HOSVD) [3]. Some other decompositions for high-order arrays exist (TUCKER1 and TUCKER2 [20], PARAFAC [1]) but will not be used here. The choice of HOSVD is motivated by the aims of providing an extension of the well-known matrix subspace technique [17,4]. The HOSVD, in its three-mode (or third order) version, decomposes the data into three orthonormal bases. This is not the case, for example, in parallel factor analysis (PARAFAC), where the array is decomposed into a sum of rank-1 arrays that may not be orthogonal one to another. This canonical decomposition is, in fact, well suited for parametric models (see [19,18,1]). In the two examples presented in Section 4, as well as in the subspace method proposed (Section 3), we do not face parametric models, and so will not use the PARAFAC model. Despite the PARAFAC model, HOSVD is not a canonical decomposition, but we will use it for the three-mode orthonormal decomposition of the array it provides. We will also show that considering the three-mode ranks provided by HOSVD (see Section 2), allows us to extend classical matrix methods to the three-way array case.

Three-mode array decomposition is always reduced to matrix computation, and computing the HOSVD of such an array is equivalent to computing the whole set of unfolding matrices that can be obtained from the original array. These unfolding matrices are close to the matrices built in the long-vector approach [16]. The non-uniqueness of long-vectors leads to a loss of information if only one special case of such a vector is considered. However, considering all long vectors enhances component recovery, and that is what we do when considering the whole set of unfolding matrices. This justifies the use of HOSVD rather than long-vectors. A theoretical proof of this, illustrated with numerical examples, is presented in Section 3. In Section 4, we present applications on real data sets from sonar with time diversity, and on a polarized seismic signal acquisition data set. Results presented in this paper are based on a previous work done by the authors [14], with some new theoretical material added.

2. Three-mode array rank definitions

After a brief recall of the three-mode array definition, we introduce some multidimensional array decompositions and link them with rank information. Such information will be exploited in Section 3 for developing a three-mode subspace technique. The two decompositions presented are the most commonly used in signal processing.

2.1. Three-mode arrays

In this paper, we will consider three-mode arrays, noted $\mathscr{Y}$, over real and complex fields. For sake of generality, definitions will be presented for the complex case and the real case will be specified when encountered.

2.1.1. Definition

A three-mode array, with dimensions N, M and P on its three modes, is given by

$$\mathscr{Y} \in \mathbb{C}^{N\times M\times P}. \tag{1}$$

The definition of the rank for such an array is the simple extension of the well-known matrix rank definition.

2.1.2. Generic rank

The *generic* rank of a three-mode array $\mathscr{Y}$ is the minimum number of rank-1 arrays that yield to $\mathscr{Y}$ by linear combination. Any three-mode array, of rank r, can be considered as

$$\mathscr{Y} = \sum_{i=1}^{r} \lambda_i \breve{\mathscr{Y}}_i, \tag{2}$$

where $\breve{\mathscr{Y}}_i$ are rank-1 unit three-mode arrays (i.e $\|\breve{\mathscr{Y}}_i\| = 1$, $\forall i$, with $\|\cdot\|$ the Frobenius norm). Any $\breve{\mathscr{Y}}_i$ can be expressed as the outer product of three unit vectors:

$$\breve{\mathscr{Y}}_i = \mathbf{u}_i \circ \mathbf{v}_i \circ \mathbf{w}_i, \tag{3}$$

where $\mathbf{u}_i \in \mathbb{C}^N$, $\mathbf{v}_i \in \mathbb{C}^M$ and $\mathbf{w}_i \in \mathbb{C}^P$ and the operator $\circ$ represents the outer product of two vectors. This rank is sometimes called *generic* rank and we will use this notation to refer to it. A more complete study of tensors rank (and especially the *generic* rank) can be found in [2]. The main problem with *generic* rank is that it can not be estimated directly [8].

2.2. Decompositions

We focus on two kinds of tensor decompositions, namely PARAFAC and HOSVD. These decompositions are of interest for the discussion as they give access to rank information that will be exploited in Section 3.

2.2.1. PARAFAC

In order to give a canonical decomposition of any given three-mode array, some techniques have been developed. A review of these techniques can be found in [3,1,10]. The PARAFAC model is well suited for parametric models, as in [19,18], and has found applications in multiway analysis [1,10,20].

2.2.1.1. Definition. The parallel factor decomposition (or canonical decomposition) of a three-mode array $\mathscr{Y} \in \mathbb{C}^{N\times M\times P}$ is a decomposition of $\mathscr{Y}$ as a linear combination of minimal number of rank-1 three-mode arrays. A schematic representation of the Parallel Factors decomposition is presented in Fig. 1.

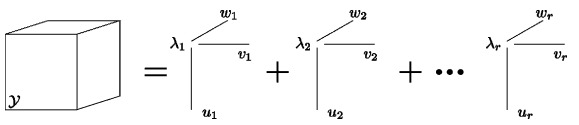

Fig. 1. PARAFAC (or canonical decomposition) of a three-mode array.

2.2.1.2. Properties. This decomposition may be seen as the generalization to the three-mode array case of the diagonalization of matrices [3]. However, the properties of this decomposition are very different from the matrix case. The most remarkable differences are:

- Rank-1 arrays of the decomposition may not be orthogonal.
- The number of terms (rank-1 three-mode arrays) in the decomposition may be superior to the largest of the three-mode dimensions, i.e. possibly $r \geqslant \max(N, M, P)$.

Other considerations about this decomposition, such as uniqueness, are not presented here and can be found in [11]. Calculation of the PARAFAC decomposition is often performed using the Alternating Least-Squares (ALS) method [10]. Another way to calculate the canonical decomposition by means of simultaneous eigen value decomposition (EVD) has been proposed in [3].

2.2.2. HOSVD

In its three-mode version, HOSVD is equivalent to the TUCKER3 model [20,10]. It was introduced by De Lathauwer [3] when dealing with independent component analysis (ICA) in the blind source separation (BSS) problem. HOSVD is a generalization of the SVD for higher order tensors. [1]

[1] A tensor of order zero is a scalar, of order one is a vector and of order two is a matrix. Higher orders are used for tensors with order higher than two. Tensors are multiway arrays that satisfy multilinearity properties.

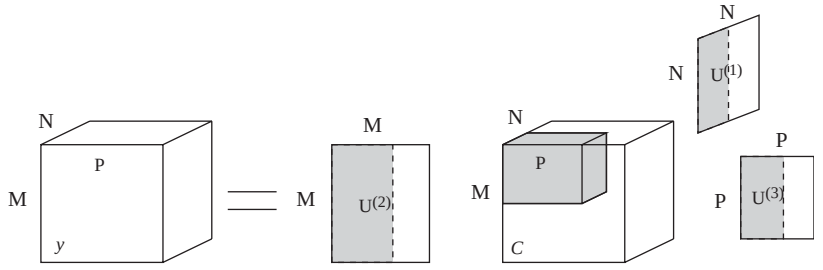

Fig. 2. HOSVD of a three-mode array ($\mathscr{Y} \in \mathbb{C}^{N\times M\times P}$).

2.2.2.1. Definition. The HOSVD of a three-way array $\mathscr{Y} \in \mathbb{C}^{N\times M\times P}$ is given by

$$\mathscr{Y} = \mathscr{C} \times_1 \mathbf{U}^{(1)} \times_2 \mathbf{U}^{(2)} \times_3 \mathbf{U}^{(3)} \tag{4}$$

with $\mathscr{C}$ the core tensor which is not hyperdiagonal but with the *all-orthogonality* property (see [3]). Matrices $\mathbf{U}^{(i)}$ contain the singular vectors along the three modes of $\mathscr{Y}$. These matrices are unitary. In (4), the notation $\times_i$ corresponds to the scalar product along the ith mode. A schematic representation of the HOSVD for a three-mode array is given in Fig. 2.

The HOSVD decomposes the original three-way array on three orthonormal bases (one for each mode). This orthogonality justifies our choice of HOSVD for the extension of the subspace method to three-way arrays (so that the decomposition of the original data set in two orthogonal parts can be performed).

2.2.2.2. Rank of unfolding matrices. Given a three-mode array, there exists three unfolding matrices that can be derived from it. So, for any $\mathscr{Y} \in \mathbb{C}^{N\times M\times P}$, the unfolding matrices are given by

$$\mathbf{Y}^{(1)} \in \mathbb{C}^{N\times MP},$$

$$\mathbf{Y}^{(2)} \in \mathbb{C}^{M\times PN},$$

$$\mathbf{Y}^{(3)} \in \mathbb{C}^{P\times NM}. \tag{5}$$

Considering these three matrices, one can define three ranks: r_1, r_2 and r_3, which are respectively the ranks of $\mathbf{Y}^{(1)}$, $\mathbf{Y}^{(2)}$ and $\mathbf{Y}^{(3)}$. These ranks are called N-mode ranks. However, another definition is possible for the rank of a three-mode array, based on the rank definition of the unfolding matrices: the rank(r_1, r_2, r_3) of $\mathscr{Y}$. This definition will be used in the proposed subspace method (see Section 3).

2.2.2.3. HOSVD computation. It has been demonstrated in [3] that the estimation of the three singular matrices of a given three-mode array can be performed by the estimation of left singular matrices of the three possible unfolding matrices. This is to say that these unfolding matrices can be decomposed into:

$$\mathbf{Y}^{(i)} = \mathbf{U}^{(i)}\mathbf{C}^{(i)}\mathbf{V}^{(i)\dagger}, \tag{6}$$

where $\mathbf{U}^{(i)}$ are singular matrices of $\mathscr{Y}$ (see Eq. (4)). The core array $\mathscr{C}$ is then obtained as

$$\mathscr{C} = \mathscr{Y} \times_1 \mathbf{U}^{(1)\dagger} \times_2 \mathbf{U}^{(2)\dagger} \times_3 \mathbf{U}^{(3)\dagger}. \tag{7}$$

This computation technique, together with the definition of the rank(r_1, r_2, r_3) shows the crucial role played by unfolding matrices in the HOSVD decomposition. An important property that must be emphasized is that the HOSVD gives a *three-mode orthogonal decomposition* of the original data set. This important property will be exploited in the subspace technique developed in Section 3.

We have seen in this section that two main definitions exist that give information about the three-mode array rank. The first is the *generic* rank r of the array and the second is the rank(r_1, r_2, r_3), composed of the three N-mode ranks (ranks of unfolding matrices, i.e. $r_i = \text{rank}(\mathbf{Y}^{(i)})$). Since we want an orthogonal decomposition of the original three-mode data set, from now on, we will only consider the rank(r_1, r_2, r_3) because it is associated with the HOSVD.

3. Subspace methods based on HOSVD

In this section, we present the extension of the subspace method for three-mode arrays. The proposed

technique is based on HOSVD, because we are looking for orthogonality between subspaces. We introduce the concept of three-mode projectors and give their expressions. We focus on the wave separation problem by means of the subspace method. Next, we show that the performance in wave separation is improved when the best approximation of a three-mode array takes into account at least two unfolding matrices instead of only one matrix. Numerical results are presented to illustrate this point.

3.1. Extension of subspace method to three-mode arrays

First, we recall the subspace method for matrices before introducing its extension to the three-mode array case.

3.1.1. Subspace methods for matrices

Consider a full rank matrix $\mathbf{A}$ ($\in \mathbb{C}^{N\times M}$ with $M \geqslant N$) and its SVD given by

$$\mathbf{A} = \mathbf{U}\mathbf{C}\mathbf{V}^{\dagger}, \tag{8}$$

where $\mathbf{U}$ and $\mathbf{V}$ contain left and right singular vectors of $\mathbf{A}$, respectively, and $\mathbf{C}$ is a pseudo-diagonal matrix containing the singular values of $\mathbf{A}$ (ordered in decreasing order). The subspace method consists in decomposing $\mathbf{A}$ into two matrices $\mathbf{A}_s$ and $\mathbf{A}_o$:

$$\mathbf{A} = \mathbf{A}_s + \mathbf{A}_o. \tag{9}$$

Matrix $\mathbf{A}_s$ is often called the *signal subspace* whereas $\mathbf{A}_o$ is called the *noise subspace*. The rank of $\mathbf{A}_s$ is denoted r and therefore, the rank of $\mathbf{A}_o$ equals $N-r$. The matrix $\mathbf{A}_s$ is considered as the best approximation of rank r of matrix $\mathbf{A}$. Eckart and Young's theorem [4] is used to obtain $\mathbf{A}_s$ by computing the best *least-squares* approximation:

$$\mathbf{A}_s = \mathbf{U}\mathbf{C}_s\mathbf{V}^{\dagger}, \tag{10}$$

where $\mathbf{C}_s$ is obtained by setting the last $N-r$ singular values to zero. It is possible to show that matrix $\mathbf{A}_s$ can be written as follows [17]:

$$\mathbf{A}_s = \mathbf{U}_s\mathbf{U}_s^{\dagger}\mathbf{A} = \mathbf{A}\mathbf{V}_s\mathbf{V}_s^{\dagger}, \tag{11}$$

where $\mathbf{U}_s$ and $\mathbf{V}_s$ are obtained by taking the r first columns of $\mathbf{U}$ and $\mathbf{V}$. The matrix $\mathbf{P}_s = \mathbf{U}_s\mathbf{U}_s^{\dagger}$ is called the projector of the *subspace signal*. Such projectors are well known and used in signal processing.

In the next paragraph, we will focus on the extension of this subspace approach to the three-mode arrays case.

3.1.2. Subspace methods for three-mode arrays

Similarly to 2D arrays, subspace methods for three-mode arrays are based on a rank approximation of the HOSVD. Consider a *full rank* (regarding the rank(r_1, r_2, r_3) definition) three-mode array $\mathscr{A}(\in \mathbb{C}^{I\times J\times K})$ and its decomposition into two three-mode arrays:

$$\mathscr{A} = \mathscr{A}_s + \mathscr{A}_o, \tag{12}$$

where $\mathscr{A}_s$ describes the *signal subspace* and $\mathscr{A}_o$ the *noise subspace*. The expression of $\mathscr{A}_s$ can be written as follows [3]:

$$\mathscr{A}_s = \mathscr{C}_s \times_1 \mathbf{U}_s^{(1)} \times_2 \mathbf{U}_s^{(2)} \times_3 \mathbf{U}_s^{(3)}. \tag{13}$$

The three-mode array $\mathscr{A}_s$ is the rank(I_s, J_s, K_s) approximation of $\mathscr{A}$. Matrices $\mathbf{U}_s^{(i)}$ are obtained by keeping the I_s (or J_s or K_s) of $\mathbf{U}^{(i)}$ (i.e. the best rank I_s, J_s and K_s approximations of $\mathbf{U}^{(i)}$) defined in (4). The last step of the process is the computation of $\mathscr{C}_s$ using the following definition [3]:

$$\mathscr{C}_s = \mathscr{A} \times_1 \mathbf{U}_s^{(1)\dagger} \times_2 \mathbf{U}_s^{(2)\dagger} \times_3 \mathbf{U}_s^{(3)\dagger}. \tag{14}$$

One can estimate the *noise subspace*, $\mathscr{A}_o$, by the substitution of the *signal subspace* from the original data set. It should be noted that such an approximation is not always the best approximation (in the mean square sense), despite the bidimensional case. However, a best rank approximation can be computed. For more details about this subject, see [3]. By combining Eqs. (13) and (14), $\mathscr{A}_s$ can be rewritten as

$$\mathscr{A}_s = \mathscr{A} \times_1 \mathbf{U}_s^{(1)}\mathbf{U}_s^{(1)\dagger} \times_2 \mathbf{U}_s^{(2)}\mathbf{U}_s^{(2)\dagger} \times_3 \mathbf{U}_s^{(3)}\mathbf{U}_s^{(3)\dagger}. \tag{15}$$

This last equation is interesting because it allows us to introduce the projectors of the three-mode array. Actually, the matrices $\mathbf{P}_i = \mathbf{U}_s^{(i)}\mathbf{U}_s^{(i)\dagger}$ are the projectors of the three unfolding matrices. Eq. (15) allows us to extend the subspace method to three-mode arrays. It must be noted that this approach consists of working in the three modes at the same time.

Nevertheless, the idea of performing the algorithm after unfolding the three-mode array in one direction is not new [16]. However, the HOSVD seems to be more interesting because all the unfolding matrices are treated at the same time. We show in the next paragraph that wave separation via the HOSVD is more efficient.

3.2. Contribution of the second unfolding matrix for wave separation

First, we show by a theoretical approach that wave separation is more efficient when the algorithm is performed with two unfolding matrices at the same time instead of using only one. The second paragraph presents a simulation to demonstrate the performance. The last paragraph presents another way to show this point.

3.2.1. Theoretical approach

We consider two wave separation algorithms based on HOSVD: the first one only uses the first unfolding matrix, whereas the second one uses the first two unfolding matrices. We want to show that the second algorithm is more efficient than the first one because it uses both directions at the same time.

We denote by $\mathscr{A}_1$ the three-mode array built with a projection only on the first mode and $\mathscr{A}_{12}$ the one built by projections on the first and the second modes. The expressions are written as follows:

$$\mathscr{A}_1 = \mathscr{A} \times_1 \mathbf{U}_s^{(1)}\mathbf{U}_s^{(1)\dagger} \times_2 \mathbf{U}^{(2)}\mathbf{U}^{(2)\dagger} \times_3 \mathbf{U}^{(3)}\mathbf{U}^{(3)\dagger},$$

$$\mathscr{A}_{12} = \mathscr{A} \times_1 \mathbf{U}_s^{(1)}\mathbf{U}_s^{(1)\dagger} \times_2 \mathbf{U}_s^{(2)}\mathbf{U}_s^{(2)\dagger} \times_3 \mathbf{U}^{(3)}\mathbf{U}^{(3)\dagger}. \tag{16}$$

The vector space described by three-mode arrays can be considered as a Hilbert space [3] and it is possible to introduce the scalar product as well as the collinearity concept between two three-mode arrays.

So, if both three-mode arrays $\mathscr{A}_1$ and $\mathscr{A}_{12}$ described by Eq. (16) are collinear, that means that the information contained in both arrays is identical. The result of wave separation with the two approaches would then be the same. On the other hand, if $\mathscr{A}_1$ and $\mathscr{A}_{12}$ are not collinear, then the information contained in both arrays is different. As $\mathscr{A}_1$ is a particular case of $\mathscr{A}_{12}$, it means that this last array contains more information, and so, it could be more interesting for wave separation. The aim of this paragraph is to show that these two arrays are not collinear.

We can write the Cauchy–Schwartz relation:

$$\langle \mathscr{A}_1, \mathscr{A}_{12} \rangle^2 \leqslant \|\mathscr{A}_1\| \cdot \|\mathscr{A}_{12}\|. \tag{17}$$

Equality is obtained when both three-mode arrays are collinear. We try to find the conditions for equality in (17). Using Eqs. (16), we can write Eq. (17) as follows (equality case):

$$\begin{aligned}\langle \mathscr{A}, \mathscr{A} \times_1 \mathbf{U}_s^{(1)}\mathbf{U}_s^{(1)\dagger} \times_2 \mathbf{U}_s^{(2)}\mathbf{U}_s^{(2)\dagger} \times_3 \mathbf{I}_3 \rangle^2 \\ = \langle \mathscr{A}, \mathscr{A} \times_1 \mathbf{U}_s^{(1)}\mathbf{U}_s^{(1)\dagger} \times_2 \mathbf{U}_s^{(2)}\mathbf{U}_s^{(2)\dagger} \times_3 \mathbf{I}_3 \rangle \\ \cdot \langle \mathscr{A}, \mathscr{A} \times_1 \mathbf{U}_s^{(1)}\mathbf{U}_s^{(1)\dagger} \times_2 \mathbf{I}_2 \times_3 \mathbf{I}_3 \rangle,\end{aligned} \tag{18}$$

where $\mathbf{I}_2$ and $\mathbf{I}_3$ are respectively the identity matrices for the second and the third mode. Thanks to this equation, we can note that equality is reached when $\mathbf{U}_s^{(2)}\mathbf{U}_s^{(2)\dagger} = \mathbf{I}_2$. This is possible only if $\mathbf{U}_o^{(2)}\mathbf{U}_o^{(2)\dagger} = 0$. That means that the *noise subspace* in the second mode does not contain energy. Otherwise, the three-mode arrays are not collinear and so the matrix built with the two first unfolding matrices is more interesting for wave separation.

We present a numerical simulation in the next paragraph to illustrate this demonstration.

3.2.2. Numerical simulations

The configuration presented in this paragraph comes from the concept of detection in the presence of reverberation with active sonar. Three echoes are collected by a linear array. In this example, we have access to several sonar images which form a three-mode array. Its structure is presented in Fig. 3. The first dimension corresponds to samples (time delay information), the second dimension to beams (angular information) and the third to sonar images (temporal diversity information). The transmitted signal is a modulated frequency (wideband signal). Two echoes are unmoving and therefore have the same positions for all sonar images whereas the third echo position changes in each sonar image.

Only four sonar images are taken into account for this simulation. Fig. 4 shows the numerical simulation output.

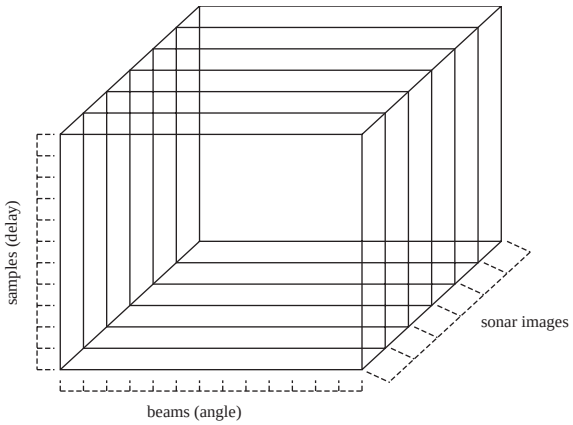

Fig. 3. Three-mode array structure.

We want to separate the two unmoving echoes from the moving one. This is impossible by a simple SVD (performed separately on each of the four images), because the power of the three echoes is the same. Using the HOSVD, however, we show that this separation is possible under some conditions.

Assume the three-mode array composed of these four sonar images is called $\mathscr{A}$. The three-mode array $\mathscr{A}_1$ is a rank approximation matrix from $\mathscr{A}$, built with only the first unfolding matrix. We want to compute the scalar product between this three-mode array and another $\mathscr{A}_{12}$ which is built with the first two unfolding matrices. At the beginning of the simulation, all singular vectors of the second unfolding matrix are taken into account. Next, less singular vectors of the second unfolding matrix are used to build the three-mode array $\mathscr{A}_{12}$. If the result is similar to the theoretical approach, the scalar product must decrease when selecting less singular vectors. Actually, it means that the *noise subspace* in the second mode becomes more important, and if the energy increases in this subspace, the scalar product between $\mathscr{A}_1$ and $\mathscr{A}_{12}$ decreases. Therefore, the result of the separation will be improved.

Fig. 5 shows the result of this simulation. At the beginning of the plot, the scalar product is important (squared norm of the three-mode array $\mathscr{A}_1$), because the two three-mode arrays are collinear. The *noise subspace* in the second unfolding matrix is empty.

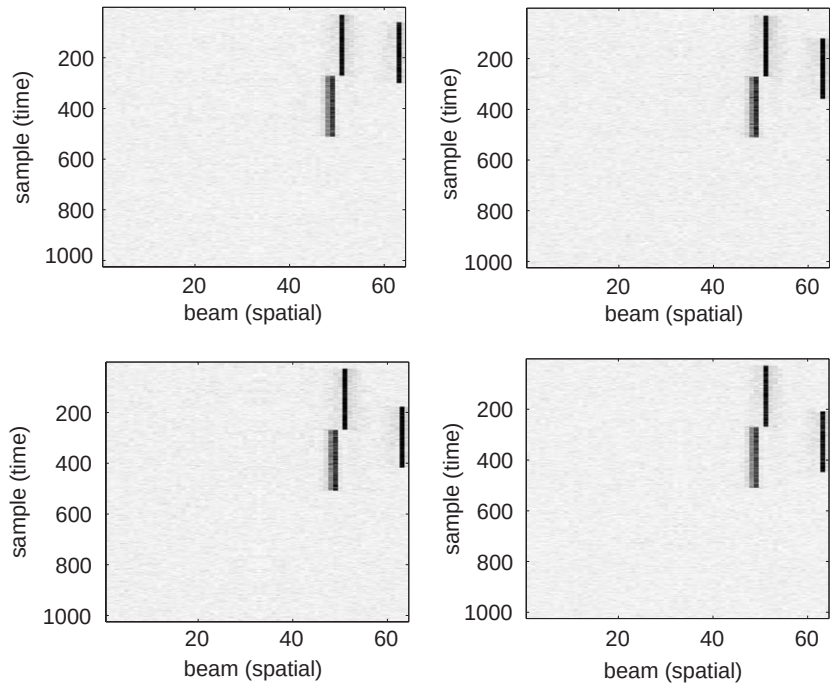

Fig. 4. Numerical simulation output.

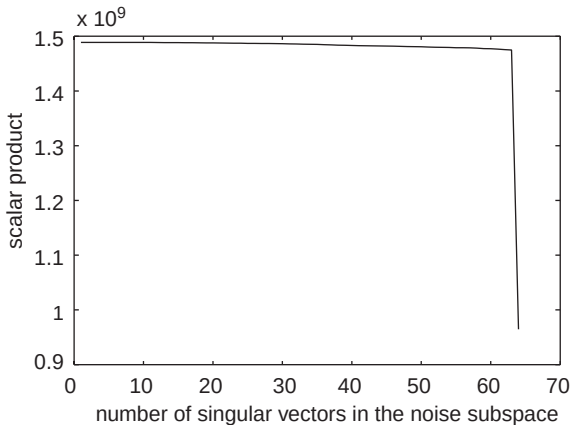

Fig. 5. Scalar product simulation.

When the *noise subspace* is built with all eigenvectors except the last, the scalar product decreases fast. Both three-mode arrays are not collinear. The separation with this last case will be better. In order to check this property, we estimate the *signal subspace* with $\mathscr{A}_1$ and $\mathscr{A}_{12}$ and compare their results. Here, $\mathscr{A}_{12}$ is built with only the last singular vectors of the second unfolding matrices. Figs. 6 and 7 show respectively the separation result by using the three-mode arrays $\mathscr{A}_1$ and $\mathscr{A}_{12}$. The first result shows that the separation is not perfect. Both signal components (unmoving and moving) are not separated whereas the subspace signal estimation is correct in the second simulation. This example shows that wave separation is more efficient if two unfolding matrices are used at the same time.

We present, in the next paragraph, another way to show this property by studying the significance of unfolding matrices.

3.2.3. Significance of unfolding matrices

We showed in the previous paragraph that wave separation is improved with the HOSVD if the *noise subspace* in the second or the third mode contains energy. We could expect this property by taking into account the structure of the unfolding matrices. Using the method described in [5], we study the rank of the unfolding matrices in simple cases. We consider three cases: an unmoving echo, an echo with a linear speed and a third one with angular speed. The third unfolding matrix is not taken into account here, because the

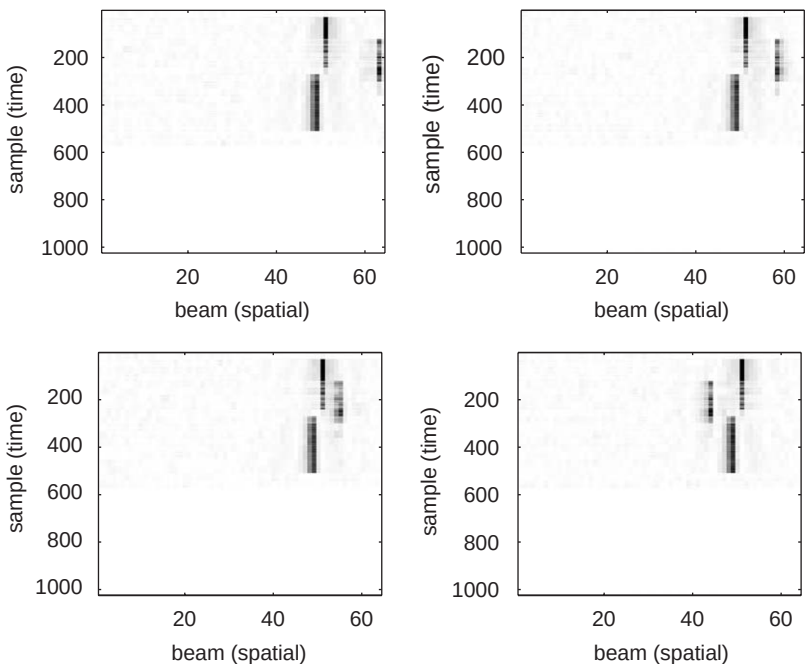

Fig. 6. Estimation of signal subspace with only the first unfolding matrix.

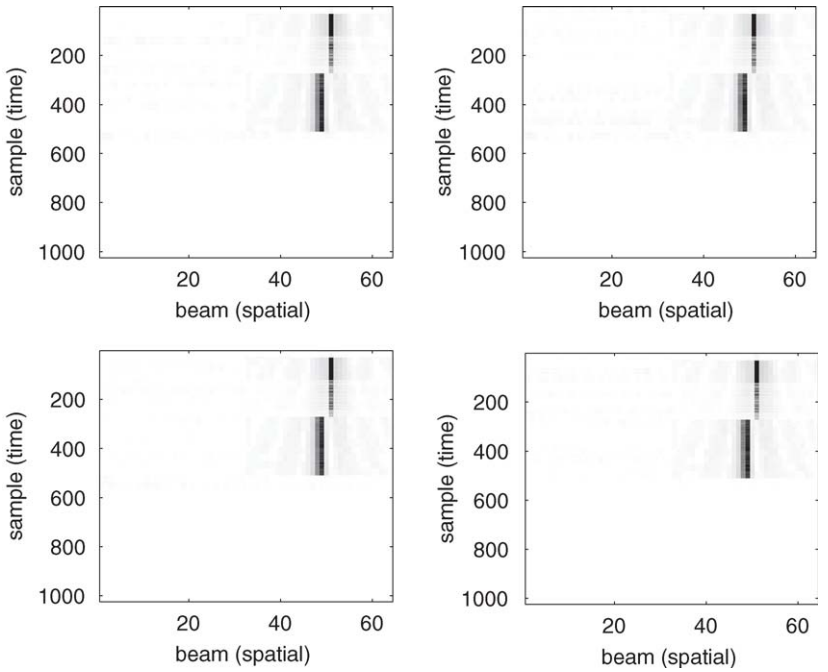

Fig. 7. Estimation of signal subspace with the first two unfolding matrices.

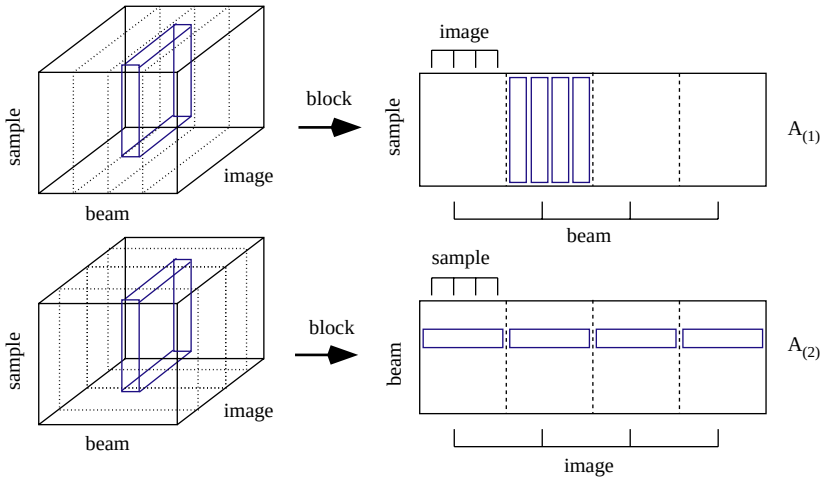

Fig. 8. Unfolding matrices for an unmoving echo.

useful signal is cut and therefore it is very difficult to interpret it.

Let us consider the first case of the unmoving echo. Fig. 8 shows it in the three-mode array as well as in the first two unfolding matrices. Only a block of the three-mode array is represented by the unfolding matrices. For the first unfolding matrix, all blue vectors are identical and therefore the rank is equal to one. For the second unfolding matrix, echoes are located on the same line (beam) and therefore the rank is also equal to one. That means that both *noise subspaces* are empty.

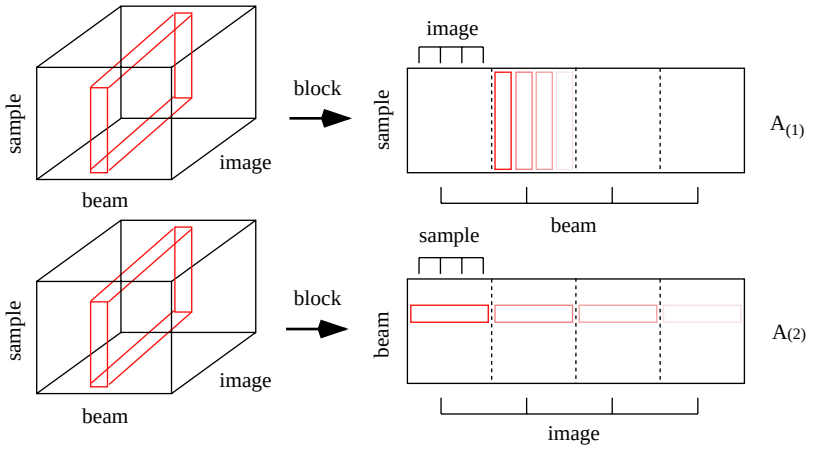

Fig. 9. Unfolding matrices for an echo with a linear speed.

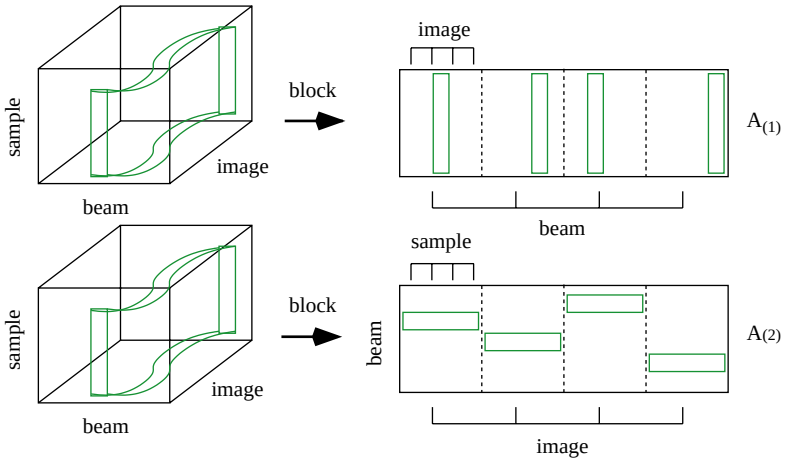

Fig. 10. Unfolding matrices for an echo with an angular speed.

Fig. 9 shows the three-mode array and the two first unfolding matrices for an echo with a linear speed. It is located in the same beam in all sonar images but its position changes in time sample. That means that the vectors in the first matrix are different. We can show [5] that the rank of this matrix is greater than one because echoes are caused by wideband signals. On the other hand, the rank of the second matrix is equal to one because the beam of the echo does not change. This result shows that the *noise subspace* in the first mode is not empty. So, the interest of the first unfolding matrix is that it can separate an unmoving echo from another echo with linear speed.

Fig. 10 shows the three-mode array and the first two unfolding matrices for an echo with angular speed. The rank of the first matrix is equal to one because all vectors are identical. But the rank of the second matrix is greater than one because several lines are filled. That means that the *noise subspace* in the second mode is not empty. Therefore, it can be used to separate an unmoving echo and an echo with an angular speed.

So, if we have no information about a moving target, it is necessary to use both unfolding matrices to be sure to separate moving from unmoving echoes. This analysis also allows better understanding of the results of the previous paragraph. Actually, when the moving

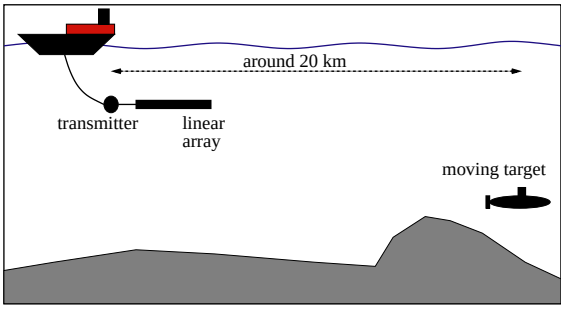

Fig. 11. Experiment description for detection in presence of reverberation.

target has only an angular speed, the separation using only the first unfolding matrix is impossible. When, both unfolding matrices are used, the separation is performed efficiently.

4. Application to real data

In this section, we present two different applications of the HOSVD subspace method described in Section 2. We consider the concept of wave separation in two different domains: active sonar (detection in presence of reverberation) and seismic signal processing.

4.1. Active sonar

We show in this section that HOSVD allows us to develop an efficient algorithm in order to detect a weak signal in the presence of reverberation. This algorithm is based on the "Principal Component Inverse" (PCI) [9,12].

4.1.1. Experiment description

The transmitted signal is hyperbolic frequency modulated (HFM) with a center frequency of 1200 Hz, a bandwidth of 100 Hz and a duration of 4 s. The array has 128 sensors with a distance between sensors of 5.2 mm. The received signal is demodulated around the center frequency and sampled at 120 Hz. Fig. 11 depicts the experiment. Reverberation is mainly due to bottom echoes.

The real target is located at several points about 20 km from the sonar transmitter. Two situations are presented: the target is located either outside or inside the reverberation. The target echo is marked by a black circle on all sonar images.

Only four recurrences are used to test the developed algorithm. Wideband beamforming as well as Spatial Block Normalized Matched Filtering (SBNMF) [5] are applied to obtain final sonar images. The SBNMF algorithm allows us to reduce the strong non-stationarity of reverberation, and therefore leads to an easier detection. Results for four recurrences are shown in Fig. 12. We can note that the detection is relatively easy in the first three recurrences. Nevertheless, some false alarms may occur (marked by a black rectangle). For the last recurrence, detection is impossible because the highest peak corresponds to a false alarm and does not come from the target echo.

4.1.2. 2D PCI algorithm and results

We present an efficient algorithm for removing the reverberation. This algorithm was first proposed in [5] and is based on PCI [9]. The PCI algorithm is a particular case of subspace methods and consists in working with the *noise subspace*.

Two hypotheses are needed for a correct running of the 2D PCI to remove reverberation:

- reverberation must be more powerful than target echoes and white noise and
- the rank of the reverberation subspace must be small.

We have shown in [5] that it is necessary to perform the PCI algorithm after wideband beamforming and before matched filtering to fulfill these hypotheses. Moreover, PCI must be applied to small blocks with respect to the transmitted signal duration. One way to cut the data set is presented in Fig. 13.

The aim of the algorithm is to decompose each matrix $\mathbf{Y}_{i,j}$ into two matrices:

$$\mathbf{Y}_{i,j} = \mathbf{Y}^{\mathrm{r}}_{i,j} + \mathbf{Y}^{\mathrm{o}}_{i,j}, \tag{19}$$

where $\mathbf{Y}^{\mathrm{r}}_{i,j}$ is built with the most important singular values and describes the reverberation subspace whereas $\mathbf{Y}^{\mathrm{o}}_{i,j}$ describes the useful signal and white noise subspace.

The most important step in this algorithm comes from the estimation of the reverberation subspace rank for each matrix $\mathbf{Y}^{\mathrm{r}}_{i,j}$. The rank is related to the useful signal power. It is estimated by computing the sum

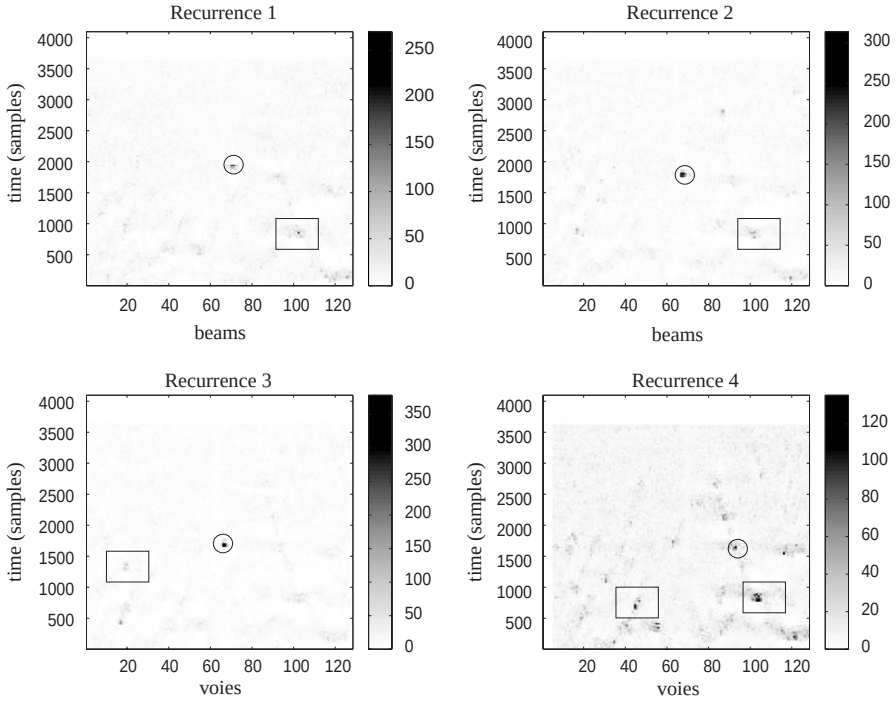

Fig. 12. SBNMF outputs for the four recurrences.

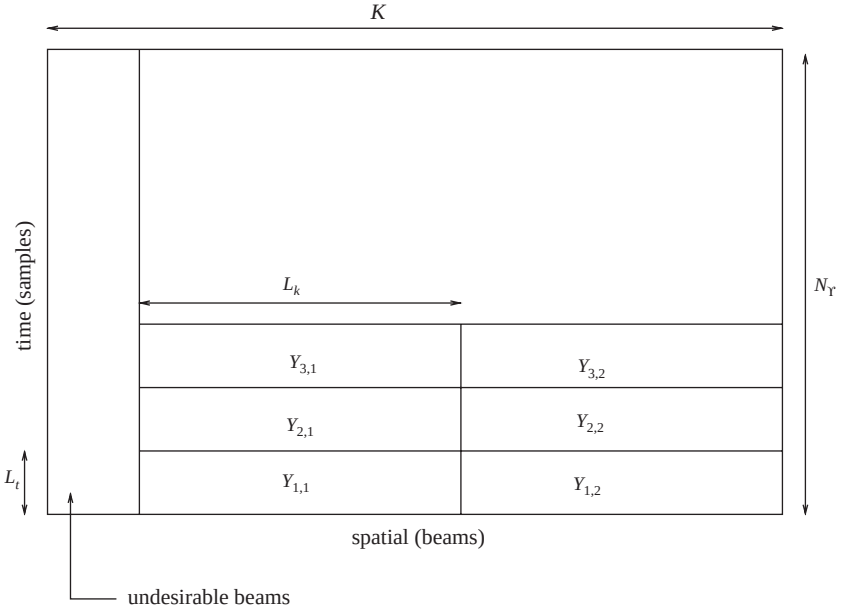

Fig. 13. Cutout of the matrix to apply the 2D PCI algorithm.

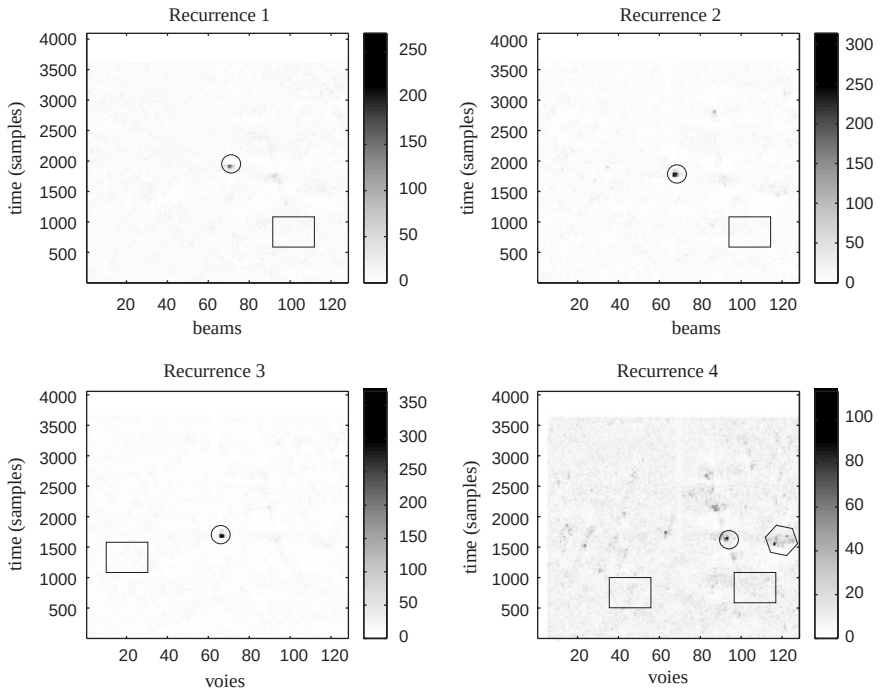

Fig. 14. SBNMF outputs after 2D PCI for four recurrences.

of the singular values of $\mathbf{Y}_{i,j}$ and comparing it to a threshold P which is linked to our prior knowledge about the target echo and the white noise power. If the sum is not greater than P, PCI does not treat the block (i,j). If there exists an index M as follows ($R_{\mathbf{Y}}$ is the rank of $\mathbf{Y}_{i,j}$):

$$\sum_{l=0}^{M} \sigma^2_{R_{\mathbf{Y}}-l} > P, \tag{20}$$

then PCI is applied to block (i,j) with a rank r equal to $R_{\mathbf{Y}}-M+1$ and the reverberation subspace is finally removed.

We apply this algorithm to our real data. The PCI algorithm is independently performed on each recurrence. The SBNMF is next applied to obtain final results which are shown in Fig. 14. We can note that the reverberation echoes marked with a black rectangle are removed by the 2D PCI. We compute the number of false alarms as a function of detection threshold to have a better idea of the detection improvement. Fig. 15 shows these results for the four recurrences. Note that 2D PCI has removed reverberation echoes for all detection thresholds (no more false alarm is located in rectangles). But, the result of the last recurrence is not sufficient for a correct detection. There remain some false alarms which are of about the same power as the target echo and therefore they are very difficult to remove with the 2D PCI. Actually, the PCI algorithm uses only the power of echoes to separate them, and so when these are close to each other, the algorithm does not run correctly.

In the next paragraph, we propose to use one more item of information to improve detection. This method is based on the HOSVD and PCI and is called the three-mode PCI algorithm.

4.1.3. Three-mode PCI algorithm

Reverberation is mainly caused by the seafloor. As the target is moving, we can say that the reverberation echoes and target echo have not the same temporal diversity. We propose to use this new contrast to separate the bottom echoes from the target echo. Actually, as real data provides four recurrences, it is possible to build a three-mode array to use the

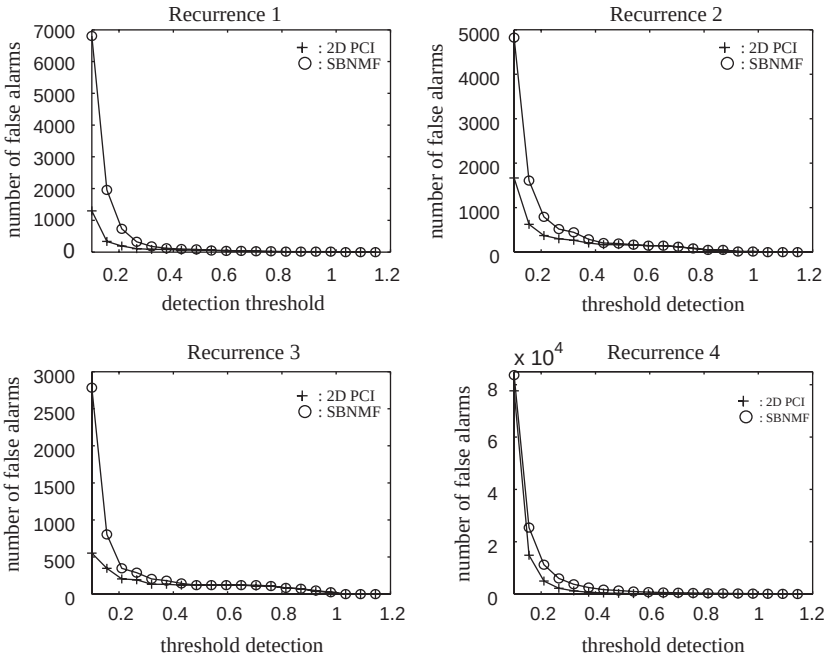

Fig. 15. Number of false alarms for SBNMF and 2D PCI.

temporal diversity information. The three-mode array has the same structure as that in Section 3.2 (see Fig. 3). Moreover, we showed in Section 3.2.3, with this kind of three-mode array, that HOSVD can separate two echoes with the same power if one of them is unmoving. As HOSVD allows us to extend subspace methods to three-mode arrays, we propose to extend the PCI to the three-mode case. This new algorithm should remove reverberation echoes which are more powerful than target echoes as well as bottom echoes, even if they have the same power as the target echo. This algorithm, called three-mode PCI, is expected to give better results compared with the 2D PCI.

From the previous analysis, we can deduce that the conditions for correct running of the three-mode PCI algorithm are:

- reverberation must be more powerful than target echo and white noise,
- reverberation echoes have to come from the bottom and the target must be moving and
- the rank of the reverberation subspace must be weak.

For the same reasons as for the 2D PCI case, it is necessary to perform three-mode PCI on small temporal blocks with respect to the transmitted signal duration. In preprocessing, wideband beamforming is applied on each recurrence. The cutout of the three-mode array is shown in Fig. 16.

In each block, PCI application needs to estimate the rank of the reverberation subspace. This estimation requires two steps as for 2D PCI. The first step consists of computing two thresholds P_1 and P_2 (for both directions) which are linked with the useful signal + white noise power but also the target movement. The second step is the rank estimation which must be made on the two unfolding matrices. For each three-mode block (i, j), the sum of squared singular values is computed and compared with the two thresholds. If there exists an index M_1 or M_2 for which:

$$\sum_{l=0}^{M_1} \sigma^2_{R_{Y_1}-l} > P_1,$$

$$\sum_{l=0}^{M_2} \sigma^2_{R_{Y_2}-l} > P_2, \tag{21}$$

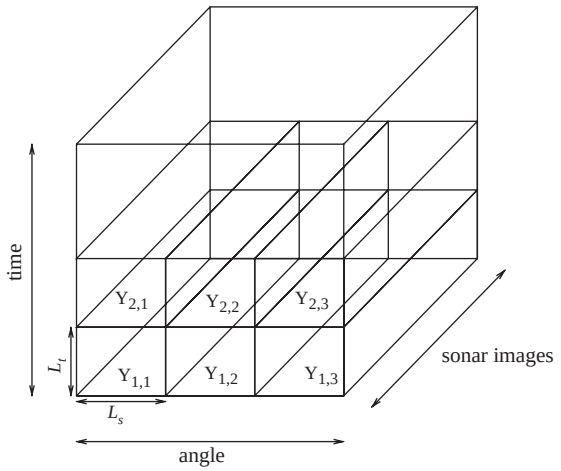

Fig. 16. Cutout of the matrix to apply the three-mode PCI algorithm.

the PCI is applied to block (i, j) with $r_1 = R_{\mathbf{Y}_1} - M_1 + 1$ and $r_2 = R_{\mathbf{Y}_2} - M_2 + 1$. Next, the reverberation subspace is computed by means of Eq. (15) and is finally removed. After this processing, the SBNMF is applied on each sonar image.

The SBNMF outputs are shown in Fig. 17. For the first three sonar images, the detection result is almost the same. On the other hand, the detection result in the last recurrence is improved. Some false alarms marked by a black hexagon have appeared. These false alarms are caused by bottom reverberation and as expected, they have been removed by three-mode PCI, even if they have the same power as the target echo.

We also show in Fig. 18 the number of false alarms as a function of the detection threshold. This allows us to compare the results of three-mode and 2D PCI approaches. For the first three recurrences, we can note that 2D PCI and three-mode PCI have the same performance, except for the first recurrence. Actually, target echo in this recurrence is less powerful and therefore it is more difficult to remove reverberation echoes with the 2D PCI. And therefore three-mode PCI removes more reverberation echoes. The most interesting result comes from the last recurrence where the number of false alarms decreases with the three-mode PCI

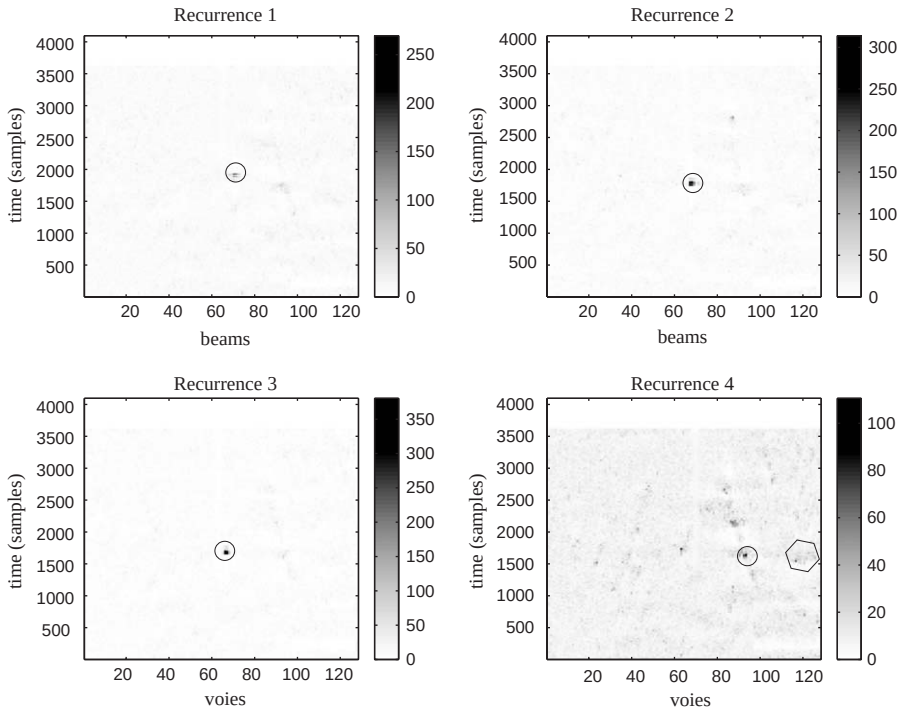

Fig. 17. SBNMF outputs after three-mode PCI for four recurrences.

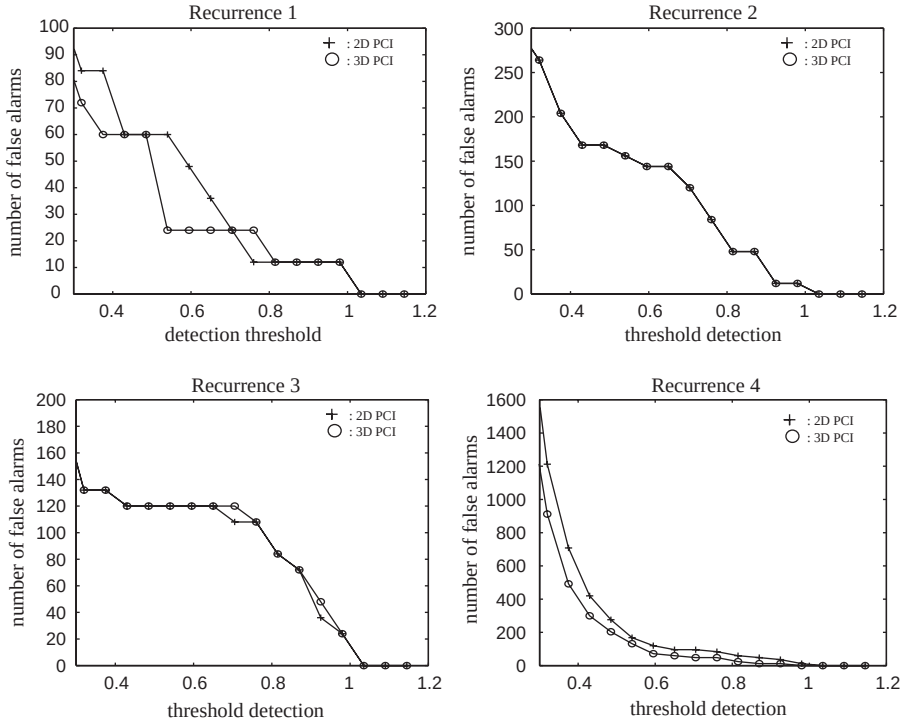

Fig. 18. Number of false alarms for 2D PCI and three-mode PCI algorithms.

for all detection thresholds. In particular, some false alarms which have almost the same power as the target echo are removed and this allows the target peak to become the highest.

This application showed the detection improvement thanks to the three-mode approach. It is possible to use more properties of different echoes in order to remove reverberation echoes. In this article, temporal diversity is used to distinguish unmoving echoes from a moving target, but there exist some other contrasts like spatial diversity to remove reverberation echoes from the sea surface.

In the next paragraph, the polarization characteristic is used to separate seismic waves.

4.2. Seismic wave separation

As shown previously (in Section 3), the use of several unfolding matrices in a wave separation problem leads to better results than a matrix approach. As HOSVD takes into account the three possible unfolding matrices in the process, wave separation on the three-way data set will be enhanced when using the HOSVD approach. We present an example of seismic wave separation, in the case where an array of *four-component* sensors is used for the recording of data having three modes: a temporal mode (recording length), a distance mode (size of the array) and a polarization mode (number of components for each sensor).

In this example, we consider the data set collected by an ocean bottom cable (OBC). Such a cable is made of *four-component* sensors that are disposed at constant spacing along the cable. Each *four-component* sensor is made of: a hydrophone, recording pressure variations, and three vector geophones recording underground displacement in three orthogonal directions (classically noted X, Y and Z). A schematic representation of a measurement process using multicomponent sensors is presented in Fig. 19.

The hydrophone provides a scalar measurement, while the set of three geophones that we call triphone

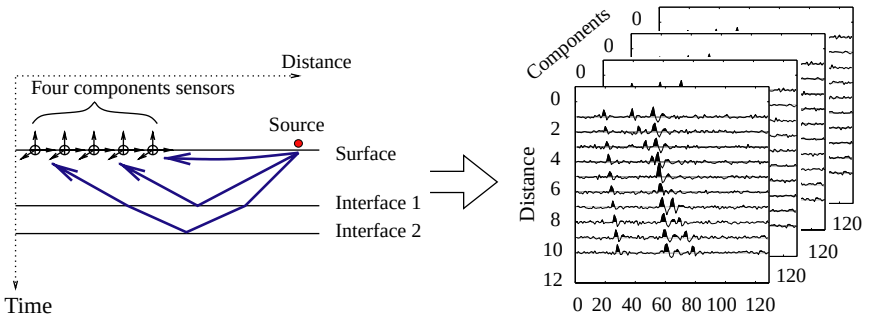

Fig. 19. Schematic representation of a multicomponent recording configuration. The data collected have three-modes: time, distance and components.

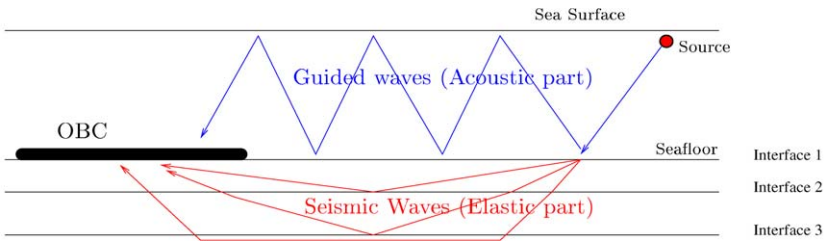

Fig. 20. Schematic representation of the waves propagation in OBC recording configuration. The acoustic guided waves propagate through the water (blue waves) and the elastic seismic waves propagates through the underground (red waves).

provides a vector measurement of the wavefield. In our example, the cable is made of 19 multicomponent sensors, which have recorded 128 time-samples on each one of their components. The cable was placed in shallow water configuration (14 m depth) and was lying on the sea floor. The source was an air gun that provided explosions. The acoustic wave generated by the source propagates through the water and, partly, through the sea floor. This last part of the wavefront must be considered as an elastic (or seismic) wave. A schematic representation of the wave propagation in an OBC recording configuration is presented in Fig. 20.

So, in the data set, there coexist waves that have been propagating through the water and waves that have been propagating through the sea floor. In order to characterize both water and ground propagations, a wave separation step is required to isolate the two sets of waves.

In Fig. 21, the original four-components of the data set are presented (a version of this figure without any notation is available: 26). One can note that a very strong dispersive wavefield (i.e. phase shift between signals recorded on two neighboring sensors) is present in the four-component signals. This is due to an acoustic wave-guide effect that may occur in shallow water configurations [6]. Water acts, in this case, as a wave-guide where acoustic waves are trapped and where several modes can propagate. The guided wavefield amplitude is amplified in the wave-guide and, therefore, a stronger magnitude than that of elastic waves is recorded.

The aim of the process is to use the whole data set simultaneously in order to separate the acoustic guided wavefield and the rest of the propagated wavefield (mainly elastic waves according to the theory [6]). In order to take advantage of a *four-component* recording campaign, we propose to use the subspace method presented in Section 3, based on HOSVD. The data set can be modeled as a three-mode array $\mathcal{Y} \in \mathbb{R}^{4\times 19\times 128}$. The subspace method, according to Eq. (8), will lead to the decomposition of $\mathcal{Y}$ into two subspaces that can

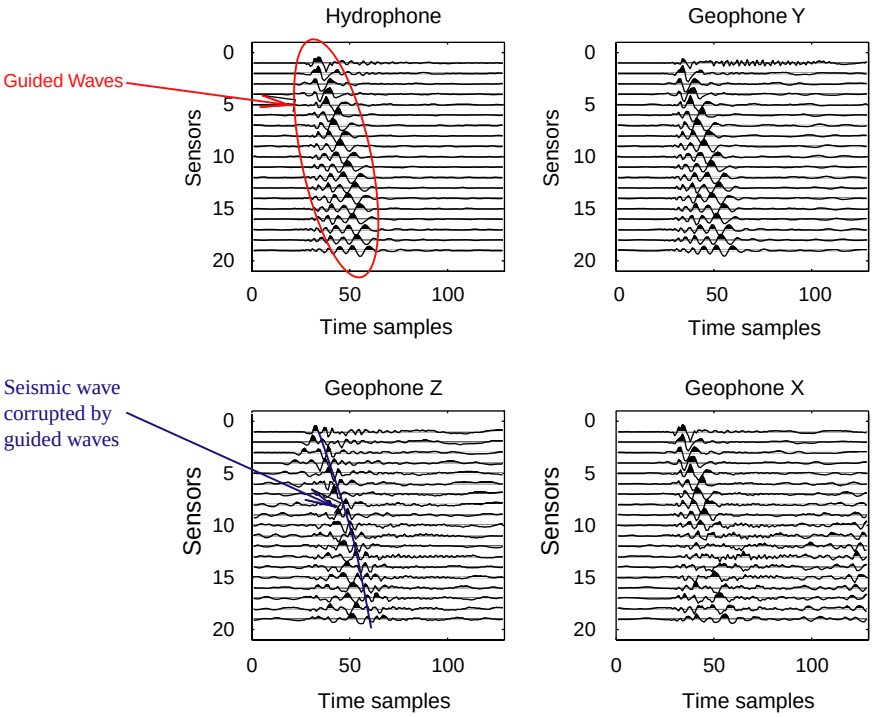

Fig. 21. Four-component of the original recorded signal. On the hydrophone components is shown the acoustic guided waves (red). On the geophone Z component is shown a reflected seismic wave (blue) corrupted by the guided waves and additional noise.

be noted as

$$\mathcal{Y} = \mathcal{Y}_1 + \mathcal{Y}_2. \tag{22}$$

This can be seen, in our special case of shallow water configuration, as a decomposition of the original data set into an *acoustic* ($\mathcal{Y}_1$) and an *elastic* part ($\mathcal{Y}_2$). The three-mode array $\mathcal{Y}_1$ is built with singular vectors associated with high magnitude singular values (in the three modes) and $\mathcal{Y}_2$ is the rest. According to physical properties of the recording waves, $\mathcal{Y}_1$ will lead to an estimate of the acoustic guided waves and $\mathcal{Y}_2$ to the elastic waves that have propagated through the ground.

$\mathcal{Y}_1$ will though be a rank(r_1, r_2, r_3) truncation of the original data set $\mathcal{Y}$. The choice of the three ranks r_i (with $i = 1, 2, 3$) is a difficult task on a real data set. In this example, we have fixed the values of the three ranks in order to get a *geophysically realistic* guided wave extraction. This means that different values have been tested for the *acoustic* part $\mathcal{Y}_1$ and looking at the results in $\mathcal{Y}_1$ and $\mathcal{Y}_2$ (in order to see if elastic coherent waves were present in the *elastic* part of the decomposition), the choice of r_i has been made. After looking at several combinations of three-mode ranks, we chose one with rank$(3, 4, 4)$. It must be pointed out that this step of determination of three-mode ranks is a drawback in the application of the proposed method to seismic data sets. This problem is directly related with the lack of power information on seismic waves. So, we are not in the same position as for the previous application (Section 4.1), where the rank of the *signal subspace* was estimated from prior knowledge. Some future work will focus on the definition of geophysical criteria in order to perform automatic determination of the N-mode ranks.

In order to compare *classical* methods with the HOSVD based one, we present results obtained using the SVD independently on the four components, and compare them to the HOSVD technique results. Our aim is to show that better results can be obtained with a three-mode array approach compared with a *component-wise* one. In our particular seismic case, working with HOSVD means that we take into

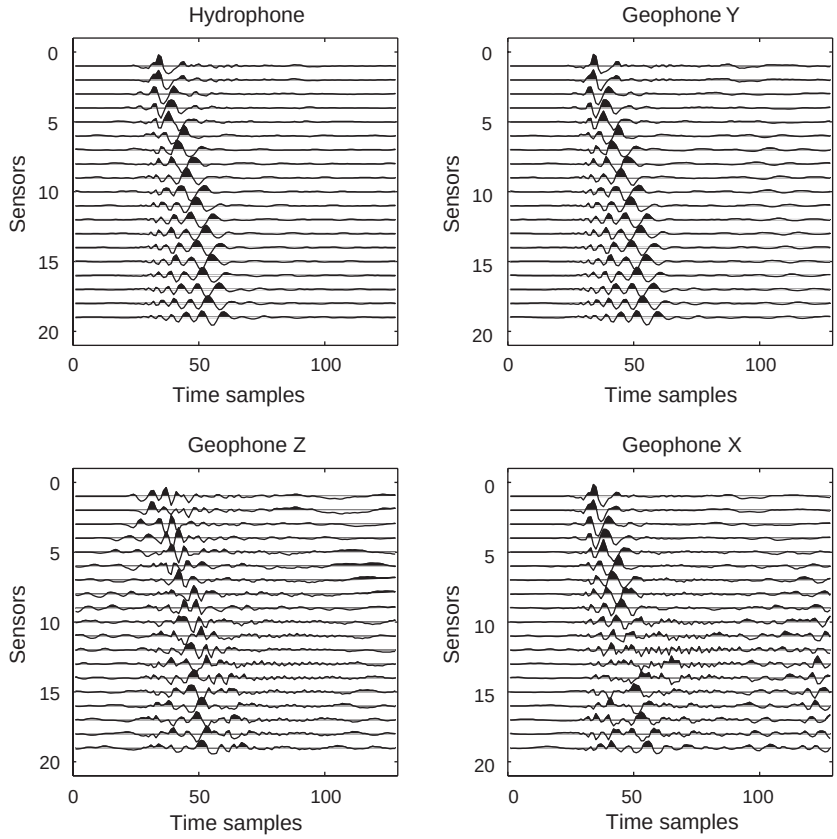

Fig. 22. Signal subspace using component-wise SVD (rank 2 truncations). This subspace is very similar to the original data set (Fig. 21).

account the relationship between components, which is in fact wave polarization (at least between the geophone components). The proposed HOSVD approach incorporates the polarization information and takes advantages of the signals redundancy on all components to evaluate it correctly on each component.

The *signal* subspace obtained with the SVD component-wise technique (i.e. the estimated acoustic part $\mathcal{Y}_1$) in Fig. 22 is presented. It can be seen that this subspace contains mainly the information that was in the original data set (Fig. 21). Inversely, in the *signal subspace* obtained with the HOSVD technique, the contribution of the acoustic wavefield is recovered on each of the four components (Fig. 23). So the *acoustic* part obtained with HOSVD contains mainly the acoustic wavefield that propagates in the water waveguide.

The difference between the results obtained with the two approaches is more significant in the estimated *noise* subspaces. When using the SVD component-wise technique, Fig. 24, the waves that remain have no geophysical significance. Especially, they do not show any coherence along the *distance* mode. On the contrary, in the *noise* subspace estimated with the HOSVD method (Fig. 25), it is possible to recover some elastic waves from the four-component signals. On the geophone Z component, it can be seen (Fig. 25) that a reflected wave may have propagated through the ground to a reflector (geological interface) before impinging on the array. This wave could already be observed on the original Z component (see Fig. 21) but was corrupted by the acoustic guided wave. Note that the SVD component-wise approach was not able to select and extract the guided

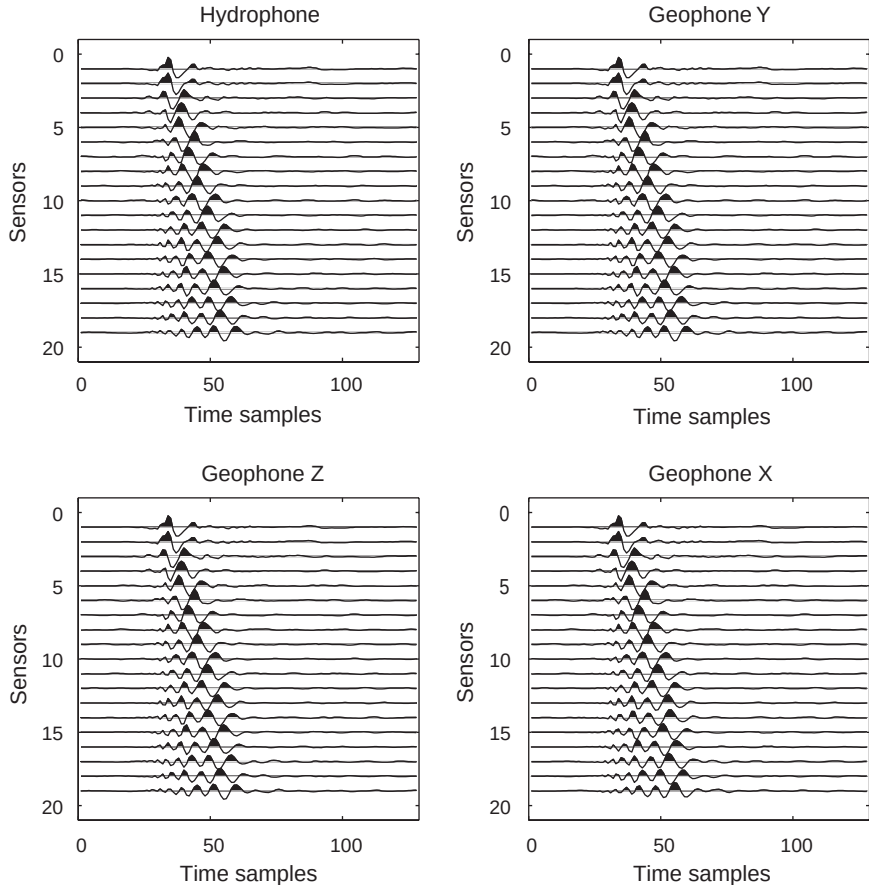

Fig. 23. Signal subspace using HOSVD (rank$(3,4,4)$ truncation). This subspace contains mainly the acoustic guided wave. HOSVD-based approach allows estimation of the four-component of the acoustic part of the wavefield.

wave contribution on this component Z (see Figs. 22 and 24).

Moreover, on the hydrophone and geophone Y components in Fig. 25, we can see some low-frequency wavefield on the right of the two images (approximately at the time-sample 100). There are also some elastic waves crossing these two *noise subspace* components from right to left (there are also some waves on the X component). These are in fact reflected waves.

A version of Fig. 25 without any notation is presented in Figs. 26 and 27. Waves are more visible in this second version of the figure.

As a conclusion on this seismo-acoustic example, we can say that the inclusion of polarization information (i.e. processing the whole components simultaneously) leads to a better separation between acoustic and elastic components. Including polarization is possible when using HOSVD (or any three-mode array model or decomposition) and leads to better results, but it is more time consuming (because it requires computation of several SVDs on the unfolding matrices). However, the improvement of the separation result makes it worth considering all components of the sensors in the processing. Moreover, polarization may be useful discriminating information between waves having similar behavior in temporal and distance mode (see [13] for examples). This information is effectively taken into account through multilinear techniques. This gives a justification for the necessary

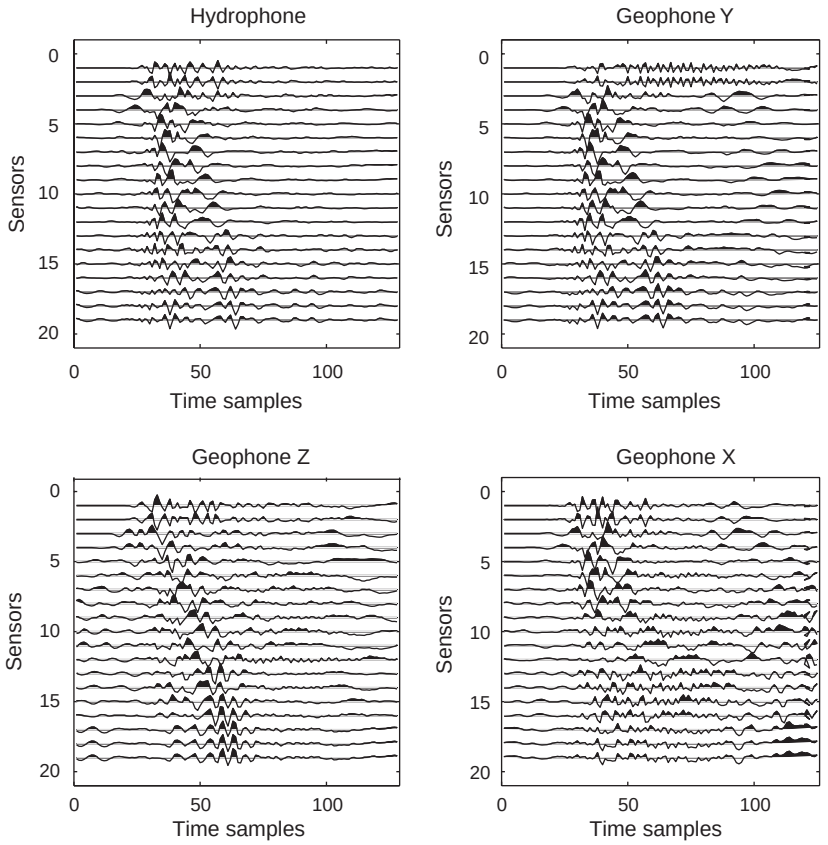

Fig. 24. Noise subspace using component-wise SVD.

use of three-mode models (rather than matrix-based models) when the data set has explicitly three modes.

5. Conclusion

In this paper we presented a subspace method for three-mode data set analysis. We also extended the subspace technique, well known for matrices, to its counterpart in the three-mode array case. Through simulation results, the utility of considering several unfolding matrices in the processing of three-mode arrays was justified. This leads us to the conclusion that some long-vector approaches can be avoided when dealing with multimode data sets, except when we consider the whole possible long-vector formulation. This last case is equivalent to the use of HOSVD. This multilinear algebra tool is the best suited to develop an extension of the subspace method according to a simple consideration: HOSVD provides an orthogonal subspace decomposition of the original three-way data set. This is convenient to extend the concept of orthogonality between the subspaces (*signal* and *noise*) built, and so, to perform *second-order* (or decorrelation)-based separation.

A problem encountered when considering multiway arrays is the concept of rank. The approach proposed in this paper is not based on *generic rank* but on three-mode rank considerations. So, the *signal* subspace in the higher-order subspace method is the rank(r_1, r_2, r_3) truncation of the original three-way array. The choice of working with three-mode rank instead of *generic* rank is also motivated by the fact that this last rank can be used when considering

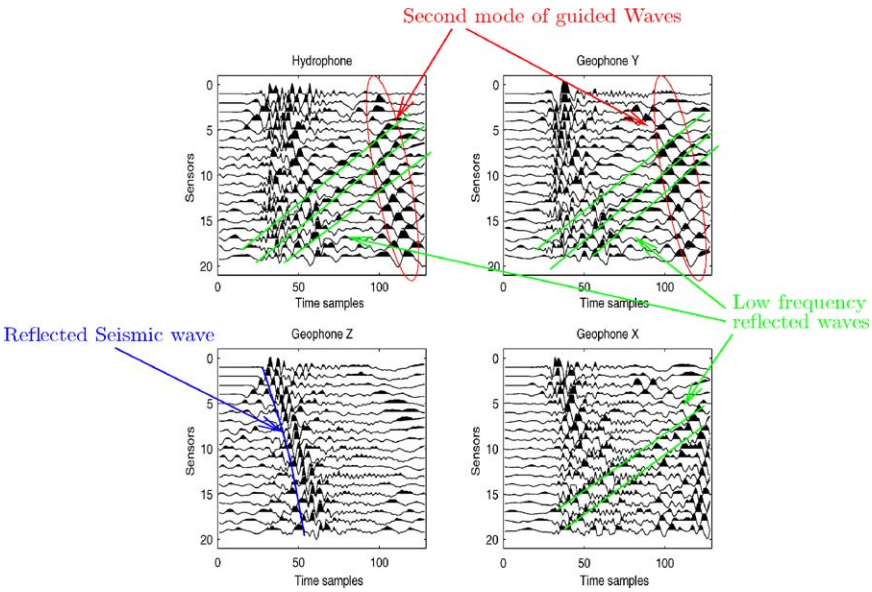

Fig. 25. Noise subspace using HOSVD. Different seismic waves are highlighted. The waves that are emphasized with colors were not recoverable with a component-wise approach. One can see in this subspace a second mode of acoustic waves (red), the reflected wave on the Z geophone component (blue) and low-frequency reflected waves (green). In order to make possible a more clear visualization of waves, we present here versions of Figs. 21 and 25 without notations: Figs. 26 and 27.

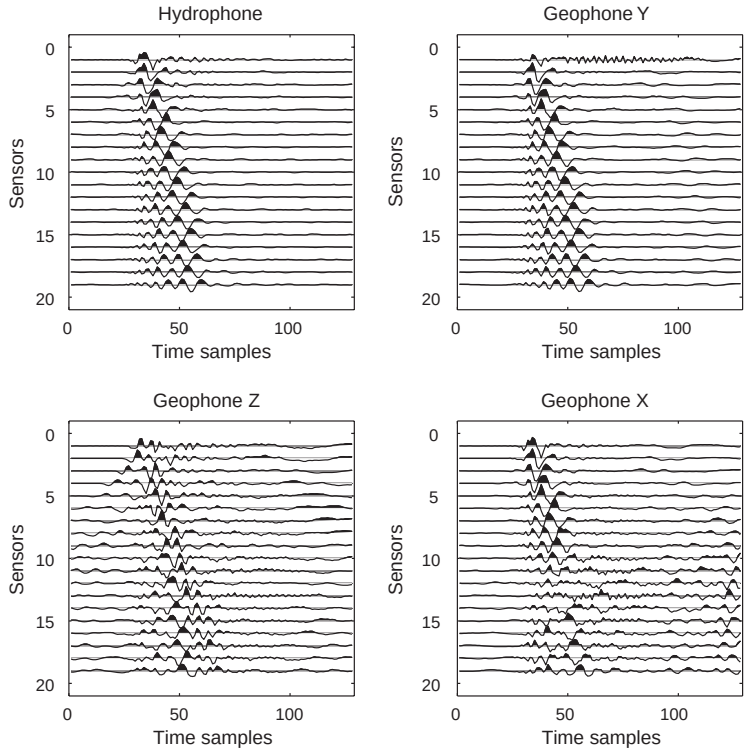

Fig. 26. Original four-component of the data set.

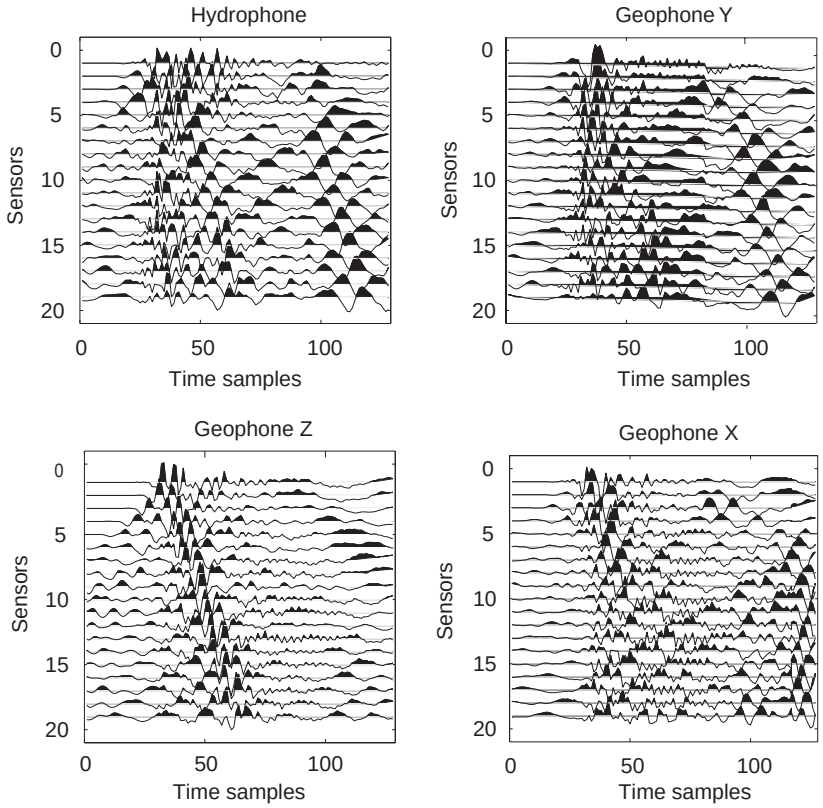

Fig. 27. Noise subspace using HOSVD.

models such as PARAFAC. This model has not been selected for the higher-order subspace method because of the possible non-orthogonality between the decomposition elements. This emphasizes the ambiguity in extending the concept of subspace method from matrix to three-way arrays: in three-way array case, *generic* rank and orthogonality do not come together as they do in the matrix case.

The application of the proposed subspace method has been presented on two kinds of data set. On three-mode sonar data, it was shown that considering all modes of the data set leads to better results than considering only two of them. An extension of the PCI algorithm has been proposed for 3D sonar images, named 3D PCI. Its efficiency was shown in the context of detection in the presence of reverberation. As a second example, we considered the context of seismo-acoustic wave separation.

In a marine seismic campaign configuration, the acoustic and seismic wavefields coexist and it was shown that taking polarization information into account leads to good wave separation performance. Polarization is though considered as the third mode of the data set which allows separation of acoustic and seismic waves, in a better way than a component-wise approach.

In our opinion, the use of multilinear tools is necessary for data set having naturally three-modes. Future work would consist of extending this approach and developing other signal processing methods for multiway data. Definition of new wave separation techniques based on multilinear algebra and proposition of new representation tools for multiway data will be a natural continuation of the presented work. The proposed higher-order subspace method can be easily applied to multiway data sets of other application

domains of signal processing, such as in electromagnetics, speech or communications. Finally, it should be noted that the subspace method has been presented for three-way arrays, but its extension to N-way data sets is straightforward.

References

[1] R. Bro, Multi-way analysis in the food industry, Models, algorithms and applications, Ph.D. Thesis, University of Amsterdam, 1998.
[2] P. Comon, Tensors decompositions, State of the art and applications, IMA Conference of Mathematics in Signal Processing, Warwick, UK, December 18–20, 2000.
[3] L. De Lathauwer, B. De Moor, J. Vandewalle, A multilinear singular value decomposition, SIAM J. Matrix Anal. Appl. 21 (4) (2000) 1253–1278.
[4] C. Eckart, G. Young, The approximation of one matrix by another one of lower rank, Psychometrica 1 (1936) 211–218.
[5] G. Ginolhac, G. Jourdain, Principal component inverse algorithm for detection in presence of reverberation, IEEE J. Ocean. Eng. 27 (2) (April 2002) 310–321.
[6] F. Glangeaud, J.-L. Mari, J.-L. Lacoume, J. Mars, M. Nardin, Dispersive seismic wave tools in geophysics, Eur. J. Environ. Eng. Geophys. 3 (1999) 265–306.
[7] G.H. Golub, C.F. Van Loan, Matrix Computation, Johns Hopkins University Press, Baltimore, MD, 1989.
[8] J. Håstad, Tensor rank is NP-complete, J. Algorithms 11 (1990) 644–654.
[9] I.P. Kirsteins, D.W. Tufts, Adaptative detection using low rank approximation to a data matrix, IEEE Trans. Aerospace Electron. Systems 30 (1) (1994) 55–67.
[10] P.M. Kroonenberg, Three-mode Principal Component Analysis, DSWO Press, Leiden, 1983.
[11] J.B. Kruskal, Three-way arrays: rank and uniqueness of trilinear decompositions, with applications to arithmetic complexity and statistics, Linear Algebra Appl. 18 (1977) 95–138.
[12] R. Kumaresan, I.P. Kirsteins, D.W. Tufts, Data adaptive signal estimation by singular value decomposition of a data matrix, Proc. IEEE 70 (6) (June 1982) 684–685.
[13] N. Le Bihan, Linear and multilinear processing of vector signals, Application to seismic wave separation, Ph.D. Thesis, INPG, 2001.
[14] N. Le Bihan, G. Ginolhac, Subspace method for 3D arrays, Second Workshop on Physics in Signal and Image Processing (PSIP), Marseille, France, 2000.
[15] C. MacBeth, L. Xiang-Yang, Linear matrix operations for multicomponent seismic processing, Geophys. J. Int. 124 (1996) 189–208.
[16] A. Nehorai, E. Paldi, Vector-sensor array processing for electromagnetic source localization, IEEE Trans. Signal Process. 42 (2) (1994) 376–398.
[17] L.L. Scharf, Statistical Signal Processing, Addison-Wesley, Reading, MA, 1991.
[18] N.D. Sidiropoulos, R. Bro, G.B. Giannakis, Parallel factor analysis in sensor array processing, IEEE Trans. Signal Process. 48 (8) (2000) 2377–2388.
[19] N.D. Sidiropoulos, G.B. Giannakis, R. Bro, Blind PARAFAC receivers for DS-CDMA systems, IEEE Trans. Signal Process. 48 (3) (2000) 810–823.
[20] L.R. Tucker, Some mathematical notes on three-mode factor analysis, Psychometrics 31 (1966) 279–311.